Supporting Information

A photo-degradable BODIPY modified Ru(II) photosensitizer for safe and efficient PDT under both normoxic and hypoxic conditions

Yatong Peng, [a,b] Xuwen Da, [a] Wanpeng Zhou, [a,b] Yunli Xu, [a,b] Xiulian Liu, [a,b] Xuesong Wang, *[a,b] and Qianxiong Zhou*[a]

[a] Key Laboratory of Photochemical Conversion and Optoelectronic Materials, Technical Institute of Physics and Chemistry, Chinese Academy of Sciences, Beijing 100190, P. R. China.

[b] University of Chinese Academy of Sciences, Beijing 100049, P. R. China.

* Corresponding author, E-mail addresses: xswang@mail.ipc.ac.cn (X. Wang); zhouqianxiong@mail.ipc.ac.cn (Q. Zhou)

Table of Contents

1. Experimental section

Synthesis and characterization of $[Ru(dip)_2(tpy\text{-}BODIPY)]^{2+}$ (complex 1)[1]

Tpy-BODIPY ligand[2] and $[Ru(dip)_2Cl_2]$[3] were synthesized following the reported methods. ^{1}H NMR (400 MHz, $CDCl_3$) for tpy-BODIPY: δ 8.70 (s, 4H), 8.55 (s, 2H), 7.91 (t, *J* = 8 Hz, 2H), 7.38 (s, 2H), 5.99 (s, 2H), 2.58 (s, 6H), 1.53 (s, 6H). HR ESI-MS: Calculated m/z for M + H^+: 480.2166, found: 480.2154.

Under a N_2 atmosphere, $[Ru(dip)_2Cl_2]$ (100 mg, 0.12 mmol) and 26 mg tpy-BODIPY (58 mg, 0.12 mmol) were dissolved in methanol/H_2O (7:1) and refluxed at 65 °C for 10 h. After the reaction was complete, the solution was filtered and the solvent was evaporated under reduced pressure. The crude product was purified by silica gel column chromatography using CH_3CN/saturated KNO_3 aqueous solution (80:1) as the eluent. The red solid complex 1 was obtained with a yield of 52%. ^{1}H NMR (400 MHz, CD_3CN) δ 9.81 (s, 1H), 8.83 (s, 1H), 8.72 (d, J = 8.1 Hz, 1H), 8.35–8.26 (m, 2H), 8.15 (m, 4H), 8.03 (m, 2H), 7.79 (d, J = 7.1 Hz, 2H), 7.73 (m, 9H), 7.65 (d, J = 5.7 Hz, 1H), 7.63–7.55 (m, 7H), 7.53 (d, J = 7.4 Hz, 2H), 7.47 (d, J = 7.3 Hz, 2H), 7.43 (s, 1H), 7.35 (dd, J = 15.7, 5.9 Hz, 2H), 7.20 (t, J = 7.4 Hz, 1H), 7.12 (m, 2H), 6.88 (d, J = 5.5 Hz, 1H), 6.41 (s, 1H), 6.20 (s, 1H), 6.08 (s, 1H), 2.49 (d, J = 8.7 Hz, 6H), 1.73 (s, 3H), 0.96 (s, 3H). ^{13}C NMR (101 MHz, CD_3CN) δ 164.99, 159.65, 157.43, 156.97, 156.60, 156.03, 155.80, 152.23, 151.93, 151.09, 149.02, 148.87, 148.74, 147.99, 147.94, 147.73, 146.79, 146.71, 144.27, 143.23, 142.21, 137.53, 136.55, 135.67, 135.41, 135.23, 135.18, 129.89, 129.70, 129.60, 129.45, 129.37, 129.31, 129.23, 128.96, 128.88, 128.81, 128.73, 128.64, 128.31, 128.04, 127.49, 127.22, 126.00, 125.95, 125.63, 125.59, 125.53, 125.39, 125.31, 125.23, 124.31, 123.14, 122.32, 121.93, 121.75, 18.58, 14.74, 14.07, 13.53. HR ESI-MS: Calculated m/z for M^{2+}: 622.6876, found: 622.6870. HPLC purity > 95%.

Synthesis and characterization of $[Ru(dip)_2(tpy)]^{2+}$ (complex 2)

Complex 2 was synthesized with a procedure similar to that of complex 1. Yield: 86%. ^{1}H NMR (400 MHz, CD_3CN) δ 8.73 (dd, *J* = 12, 8 Hz, 2H), 8.29 (d, *J* = 4 Hz, 1H), 8.20 (m, 4H), 8.16–8.09 (dd, *J* = 8, 4 Hz, 2H), 8.02 (d, *J* = 8 Hz, 1H), 7.92 (d, *J* = 4 Hz, 1H), 7.77 (d, *J* = 8 Hz, 1H), 7.75–7.55 (m, 20H), 7.53–7.46 (m, 4H), 7.39–7.29 (m, 3H), 7.26 (d, *J* = 8 Hz, 1H), 7.08 (s, 1H), 6.92 (d, *J* = 4 Hz, 2H). ^{13}C NMR (101 MHz, CD_3CN) δ 164.99, 159.65, 157.43, 156.97, 156.60, 156.03, 155.80, 152.23, 151.93, 151.09, 149.02, 148.87, 148.74, 147.99, 147.94, 147.73, 146.79, 146.71, 144.27, 143.23, 142.21, 137.53, 136.55, 135.67, 135.41, 135.23, 135.18, 129.89, 129.70, 129.60, 129.45, 129.37, 129.31, 129.23, 128.96, 128.88, 128.81, 128.73, 128.64, 128.31, 128.04, 127.49, 127.22, 126.00, 125.95, 125.63, 125.59, 125.53, 125.39, 125.31, 125.23, 124.31, 123.14, 122.32, 121.93, 121.75, 18.58, 14.74, 14.07, 13.53. HR ESI-MS: Calculated m/z for M^{2+}: 499.6306, found: 499.6286. HPLC purity > 95%.

Theoretical calculations

All calculations were carried out with the Gaussian 09 (G09) program package 3, using the density functional theory (DFT) method with Becke's three-parameter hybrid functional and LeeYang-Parr's gradient corrected correlation functional (B3LYP).[4] The LANL2DZ basis set and effective core potential were used for the Ru atom,[5] and the 6-31 G** basis set was used for remaining atoms.[6, 7] The ground-state geometry of the complex was optimized in H_2O using the conductive polarizable continuum model (CPCM), and frequency calculation was performed to verify that the optimized structure was in an energy minimum state. The orbitals were analyzed and plotted using the Gauss View 5.0 program.

2. ^{1}H NMR, ^{13}C NMR and mass spectra

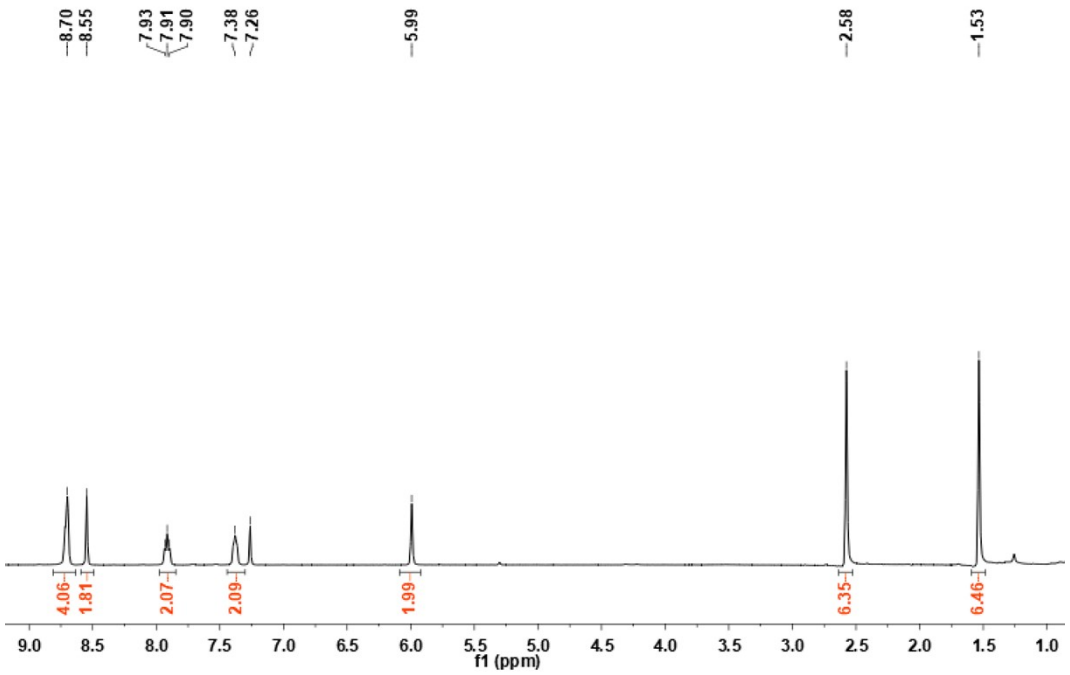

Figure S1. ^{1}H NMR spectrum of tpy-BODIPY in CD_3Cl.

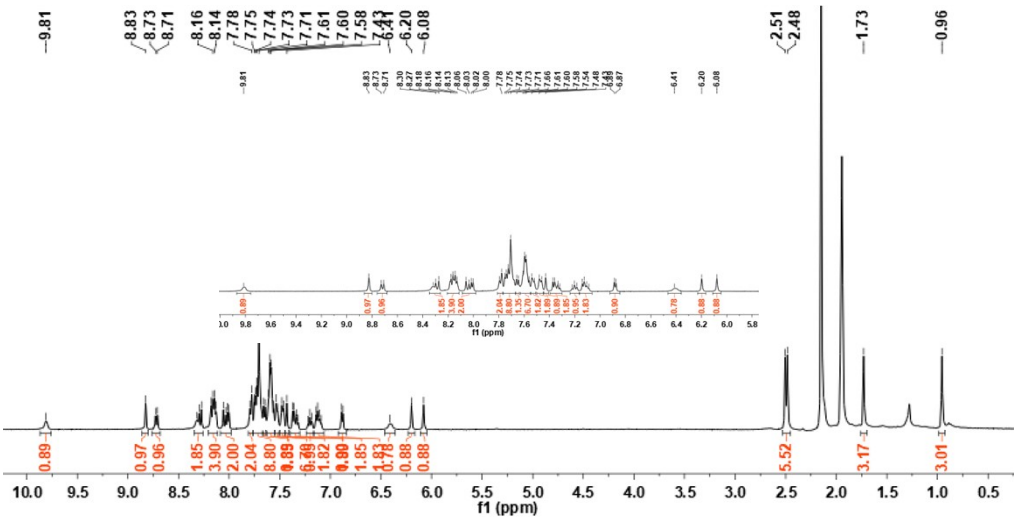

Figure S2. ^{1}H NMR spectrum of complex 1 in CD_3CN.

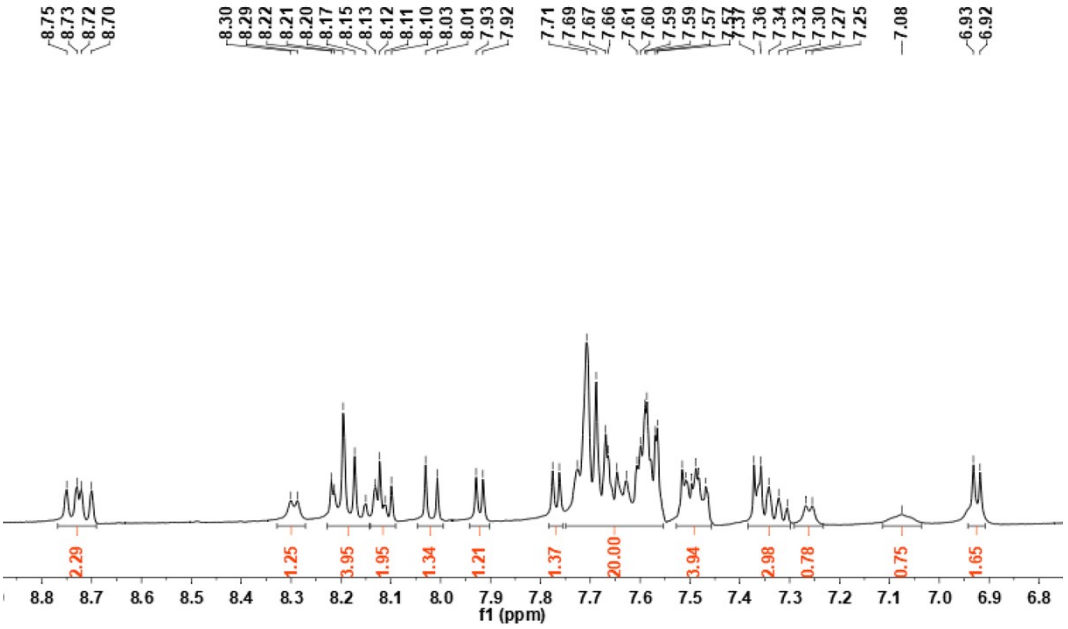

Figure S3. ^{1}H NMR spectrum of complex 2 in CD_3CN.

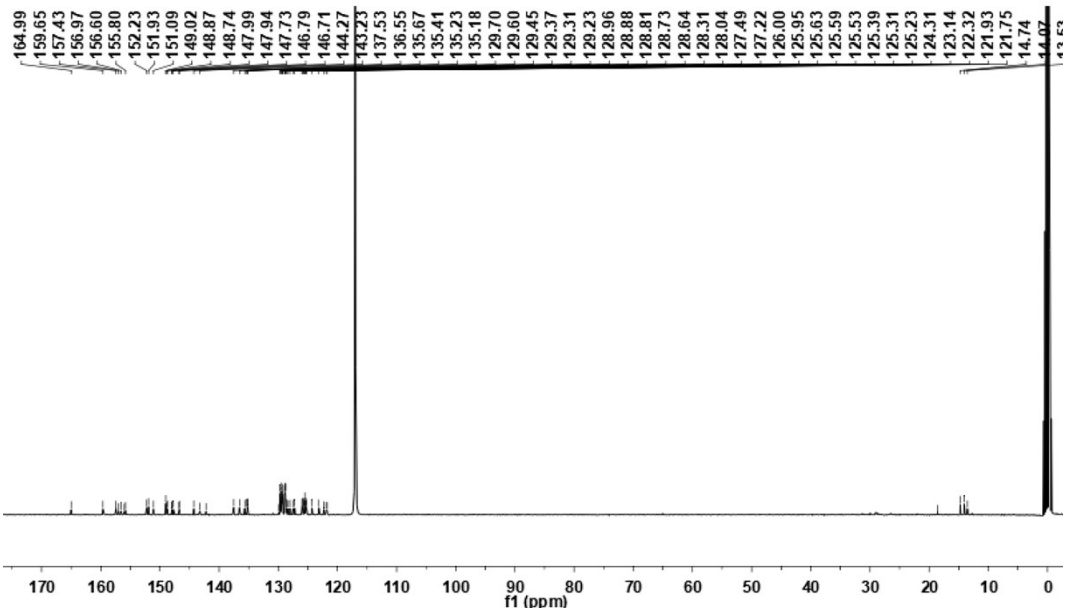

Figure S4. ^{13}C NMR spectrum of complex 1 in CD_3CN.

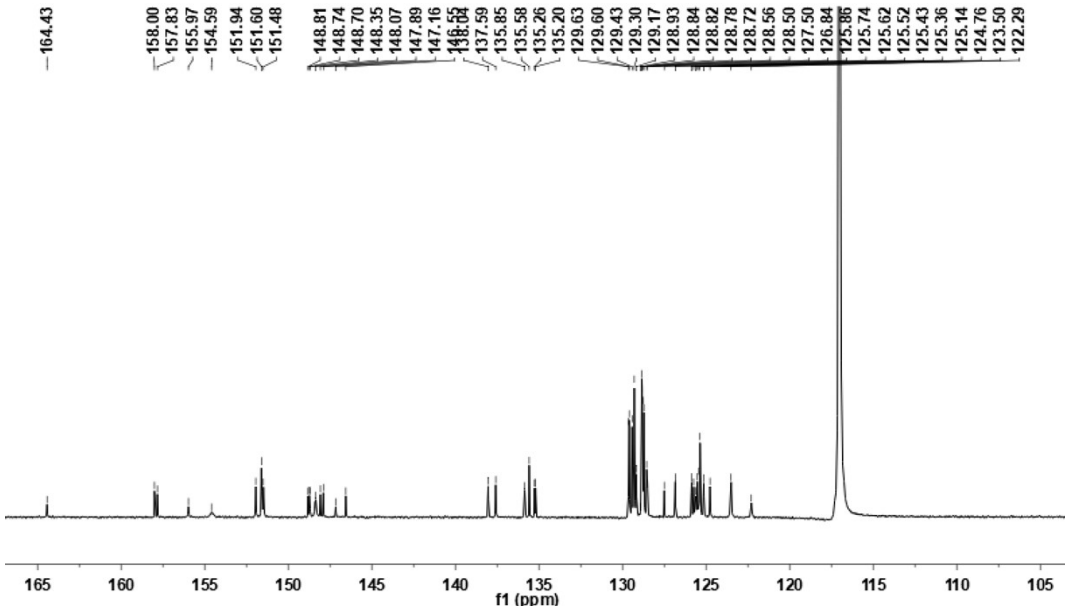

Figure S5. ^{13}C NMR spectrum of complex 2 in CD_3CN.

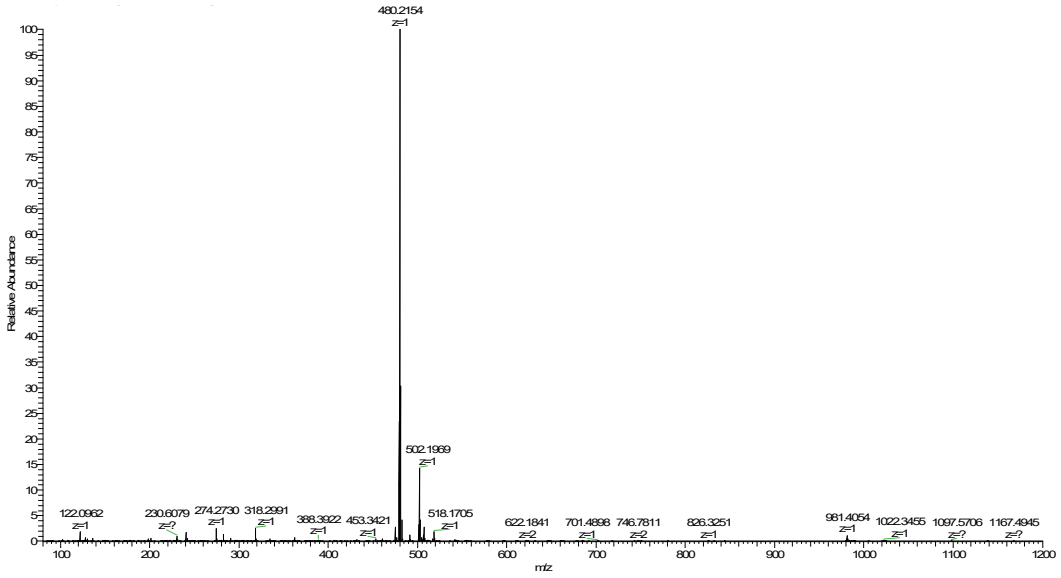

Figure S6. ESI mass spectrum of tpy-BODIPY in CH_3CN (calculated m/z for $M+H^+$: 480.2166, found: 480.2154).

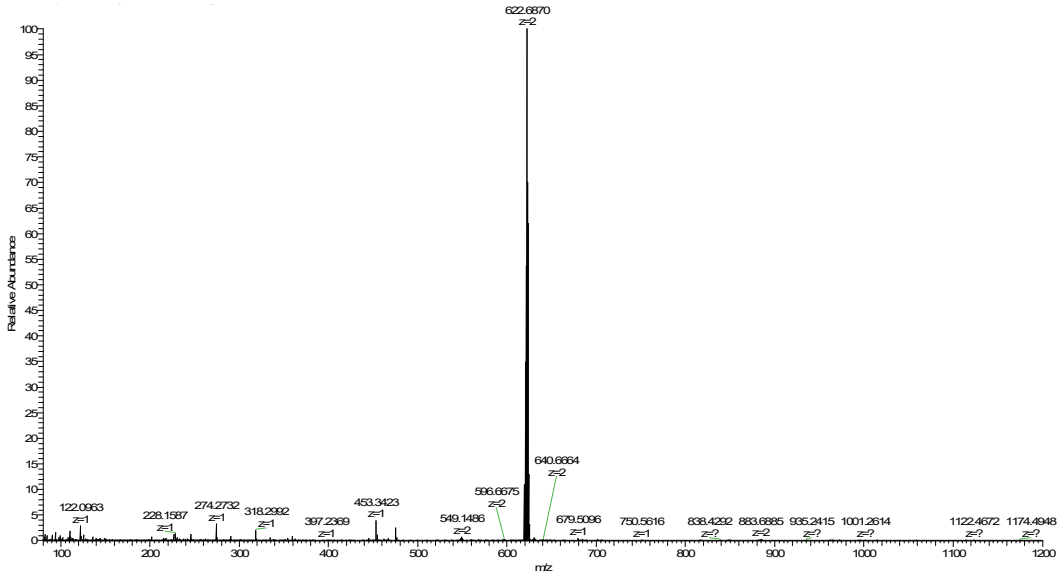

Figure S7. ESI mass spectrum of complex 1 in CH_3CN (calculated m/z for M^{2+}: 622.6876, found: 622.6870).

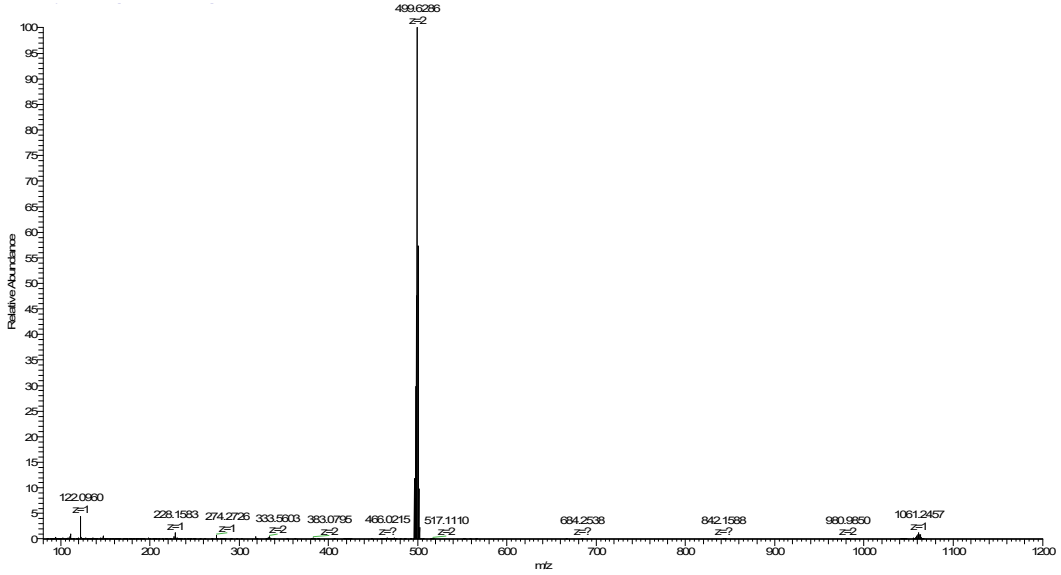

Figure S8. ESI mass spectrum of complex 2 in CH_3CN (calculated m/z for M^{2+}: 499.6306, found: 499.6286).

3. Photo-stability of complexes 1 and 2

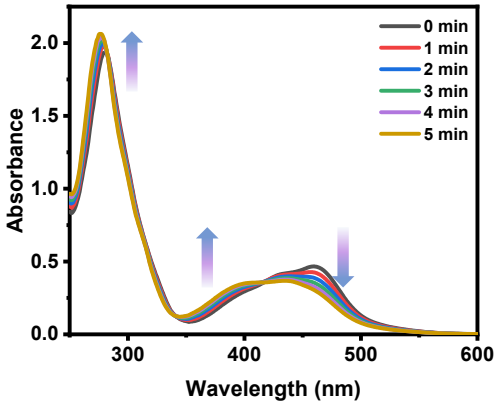

Figure S9. Absorption spectra changes of complex 2 upon irradiation (470 nm, 22.5 mW cm^{-2}) in CH_3CN.

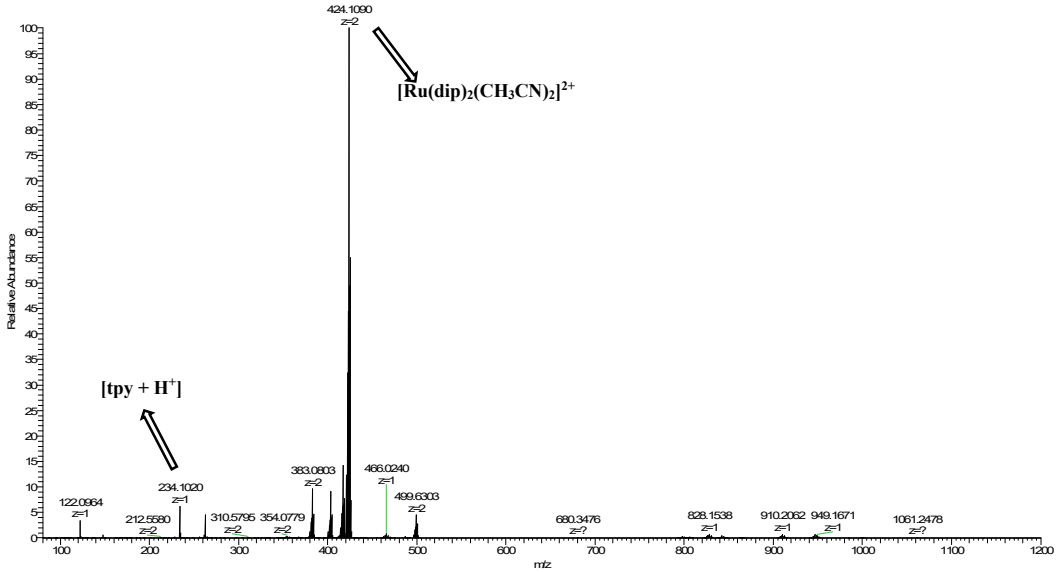

Figure S10. ESI mass spectrum of complex 2 after irradiation (470 nm, 22.5 mW cm^{-2}, 30 min) in CH_3CN. The m/z peak at 424.1090 can be ascribed to the compound that the tpy ligand was replaced by two CH_3CN. Calculated m/z for $[Ru(dip)_2(CH_3CN)_2]^{2+}$: 424.1095, found: 424.1090; Calculated m/z for $[tpy + H^+]$: 234.1031, found: 234.1020.

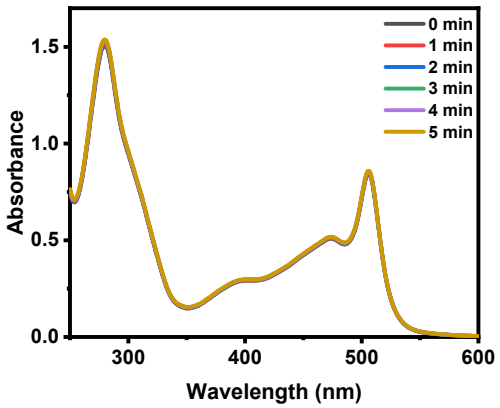

Figure S11. Absorption spectra changes of complex 1 upon irradiation (470 nm, 22.5 mW cm^{-2}) in CH_3CN.

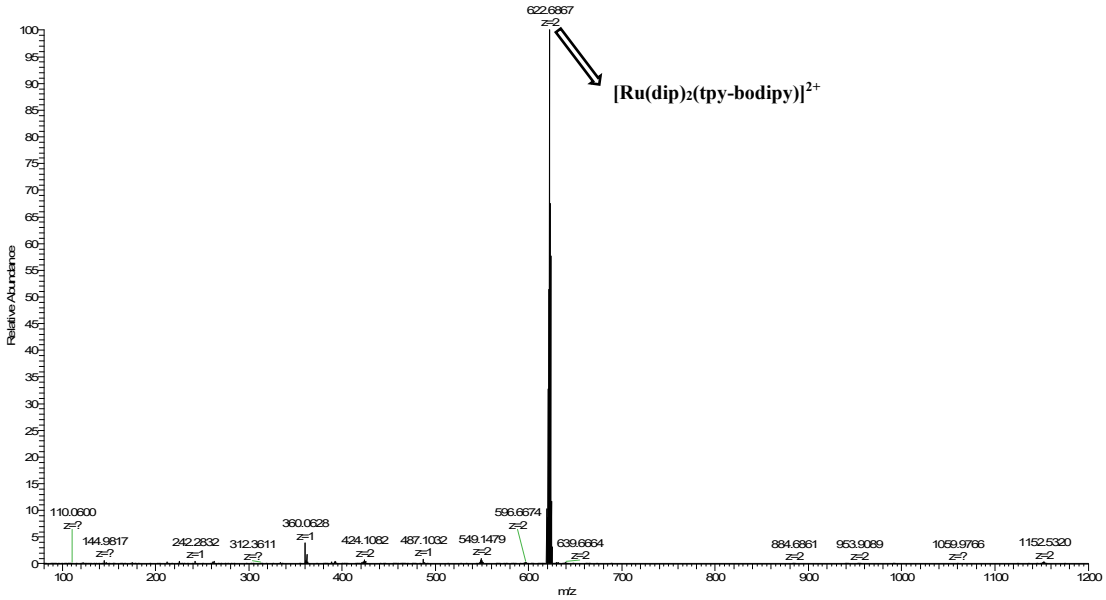

Figure S12. ESI mass spectrum of complex 1 after irradiation (470 nm, 22.5 mW cm^{-2}, 30 min) in CH_3CN. No free tpy-BODIPY ligand and $[Ru(dip)_2(CH_3CN)_2]^{2+}$ based peaks were detected.

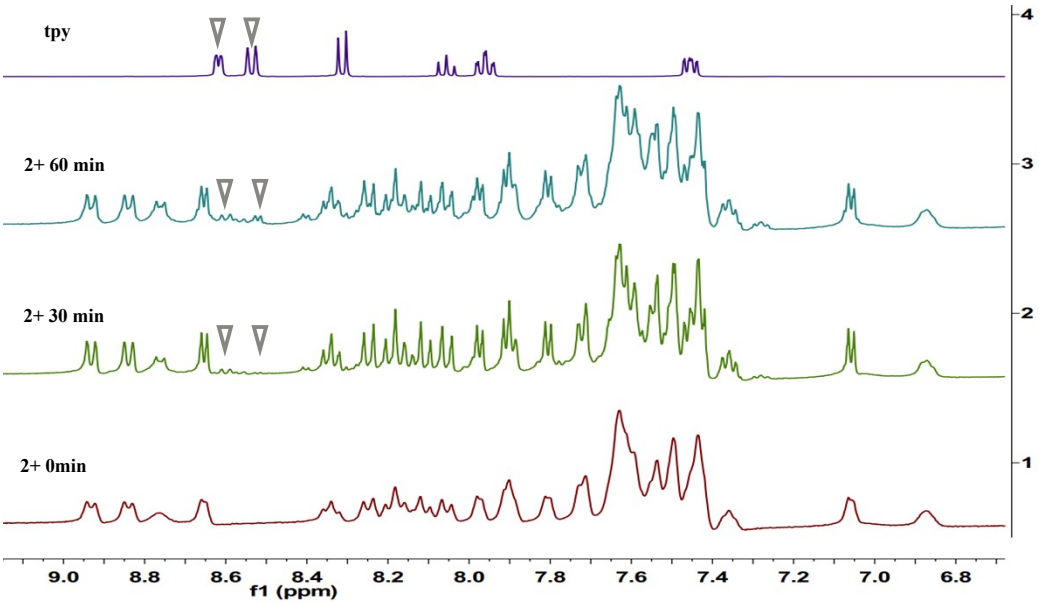

Figure S13. ^{1}H NMR spectra of complex 2 upon irradiation (470 nm, 22.5 mW cm^{-2}) with different times in CD_3COCD_3/D_2O = 2:1. The spectrum of free tpy ligand was also displayed for comparison. ▽ represents the free tpy ligand based peaks.

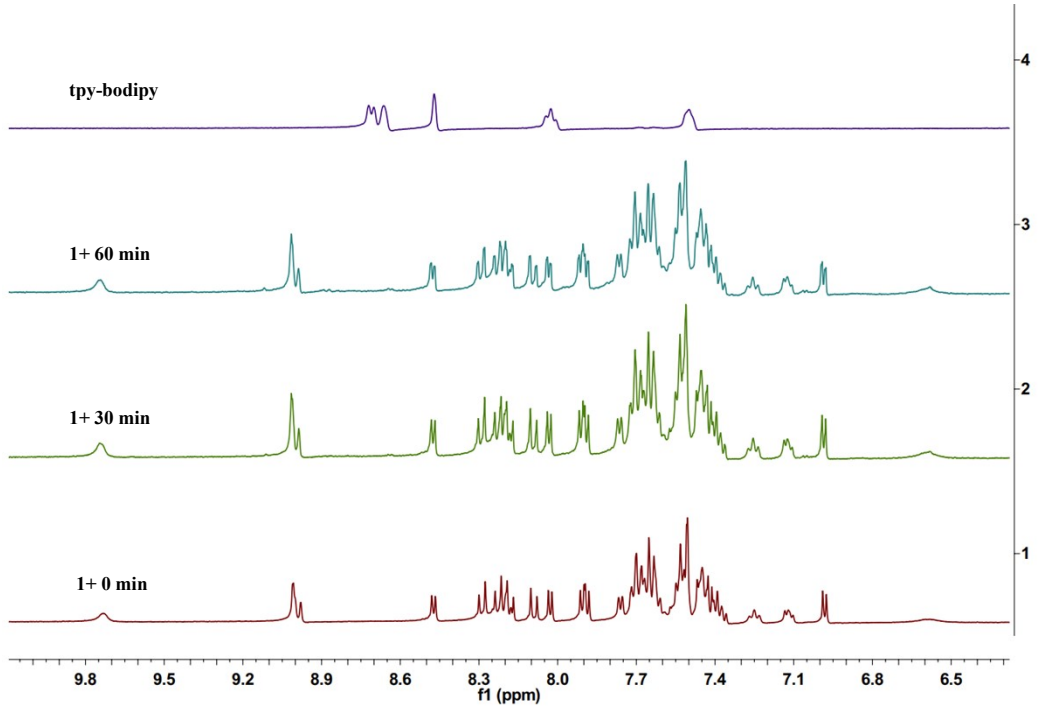

Figure S14. ^{1}H NMR spectra of complex 1 upon irradiation (470 nm, 22.5 mW cm^{-2}) with different times in CD_3COCD_3/D_2O = 2:1. The spectrum of free tpy-BODIPY ligand was also provided for comparison.

4. Theoretical calculations

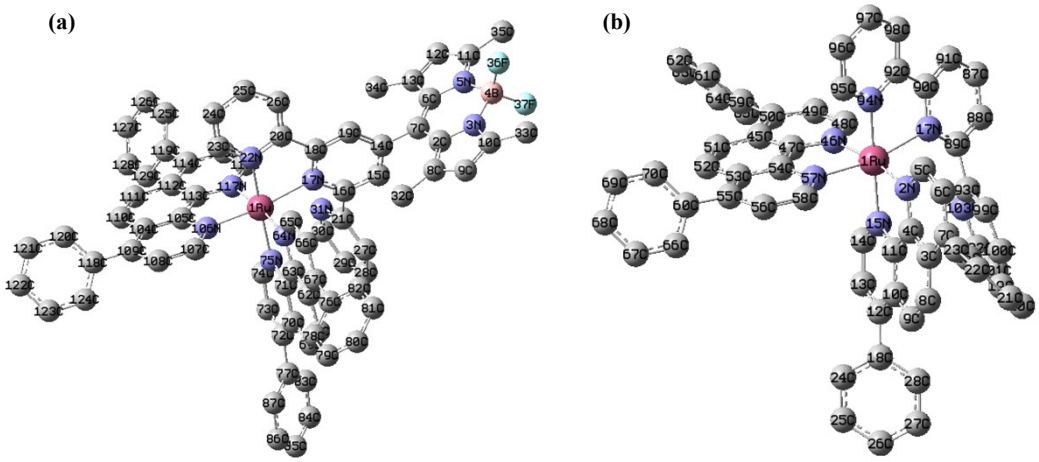

Fig. S15. The optimized structure of (a) complex 1 and (b) complex 2 based on Gaussian calculation.

Table S1. Selected bond length (Å) of complexes 1 and 2[a]

1		2	
Bond	Length	Bond	Length
1Ru-17N	2.190	1Ru-17N	2.201
1Ru-22N	2.100	1Ru-94N	2.104
1Ru-64N	2.120	1Ru-57N	2.101
1Ru-75N	2.124	1Ru-46N	2.123
1Ru-106N	2.099	1Ru-15N	2.118
1Ru-117N	2.111	1Ru-2N	2.108

[a] The data in the table were obtained by theoretical calculation.

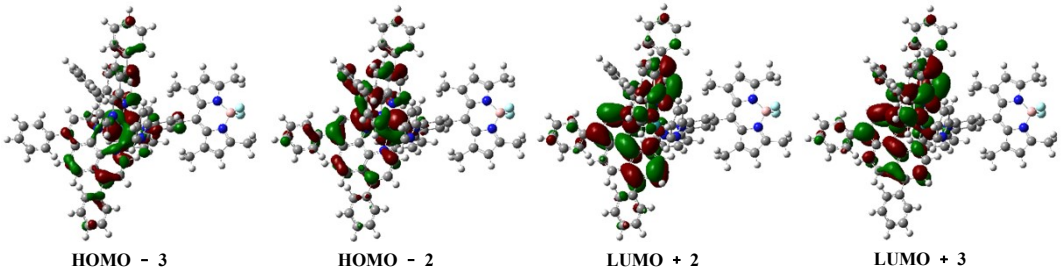

Figure S16. Other selected frontier molecular orbitals of complex 1

Table S2. Singlet state transitions of complex 1 based on TD-DFT calculation (H = HOMO, L = LUMO).

Singlet Excited state	Energy (eV)	Wavelength (nm)	Oscillator Strength(f)	Calculated transitions and Orbital contributions
S_1	2.51	494.74	0.0049	H - 1→L + 1 (86%)
S_2	2.60	476.06	0.0059	H→L + 1 (97%)
S_3	2.70	459.63	0.0045	H - 2→L + 1 (65%)
S_4	2.71	457.63	0.0022	H - 1→L + 3 (55%)
S_5	2.73	454.19	0.0071	H - 1→L + 2 (75%)
S_6	2.85	434.62	0.1328	H - 3→L + 1 (75%)
S_7	2.86	433.60	0.0682	H - 1→L (77%) H→L (20%)

Table S3. Triplet state transitions of complex 1 based on TD-DFT calculation (H = HOMO, L = LUMO).

Triplet Excited state	Energy (eV)	Wavelength (nm)	Oscillator Strength(f)	Calculated transitions and Orbital contributions
T_1	1.47	842.73	0.0000	H→L (100%) ^{3}BODIPY*
T_2	2.33	531.81	0.0000	H - 1→L + 1 (71%) ^{3}MLCT
T_3	2.42	510.94	0.0000	H - 1→L + 3 (36%)
T_4	2.45	504.87	0.0000	H - 1→L + 2 (18%)
T_5	2.49	497.42	0.0000	H - 1→L + 2 (23%)

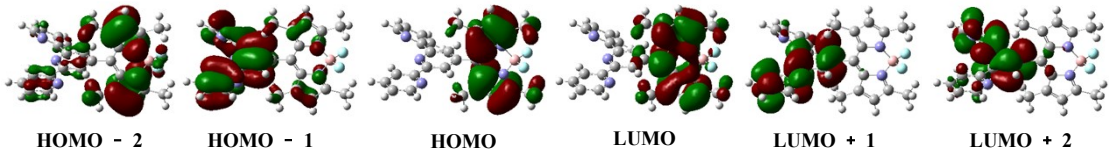

Fig. S17. Selected frontier molecular orbitals of tpy-BODIPY.

Table S4. Three minimum singlet state transitions of tpy-BODIPY based on TD-DFT calculation (H = HOMO, L = LUMO)

Singlet Excited state	Energy (eV)	Wavelength (nm)	Oscillator Strength(f)	Calculated transitions and Orbital contributions
S_1	2.90	427.72	0.5776	H→L (98%)
S_2	3.31	374.39	0.0332	H - 1→L (92%)
S_3	3.39	365.81	0.0085	H→L + 1 (98%)

Table S5. Three minimum triplet state transitions of tpy-BODIPY based on TD-DFT calculation (H = HOMO, L = LUMO).

Triplet Excited state	Energy (eV)	Wavelength (nm)	Oscillator Strength(f)	Calculated transitions and Orbital contributions
T_1	1.51	818.66	0.0000	H→L (100%)
T_2	2.71	457.11	0.0000	H - 2→L (81%)
T_3	2.89	428.62	0.0000	H→L + 2 (93%)

5. ROS generation

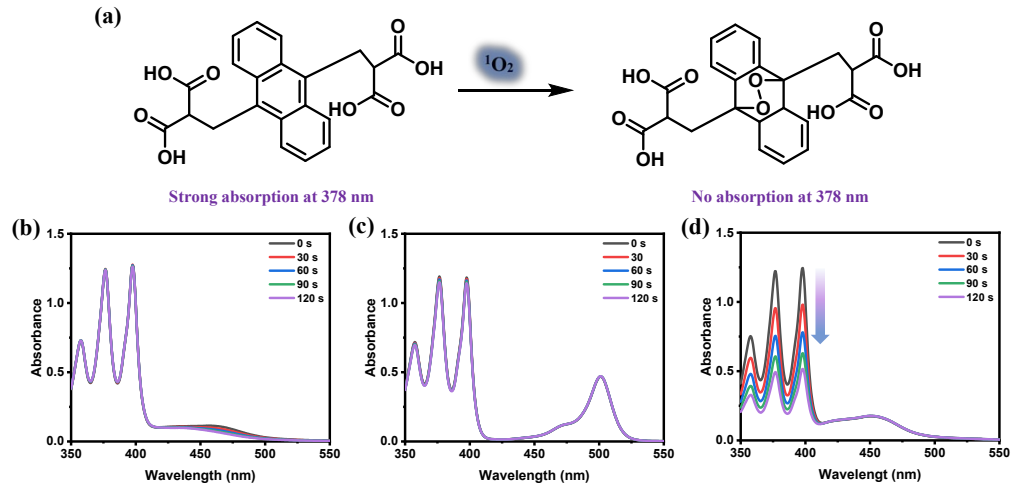

Figure S18. (a) The mechanism of 9,10-anthracenediyl-bis(methylene)-dimalonic acid (ABDA) as the $^1O_2$ probe; Absorption spectra changes of ABDA in acetonitrile upon irradiation (470 nm, 22.5 mW cm^{-2}) for different time in the presence of complex 2 (b), tpy-BODIPY (c) and $[Ru(bpy)_3]^{2+}$ (d).

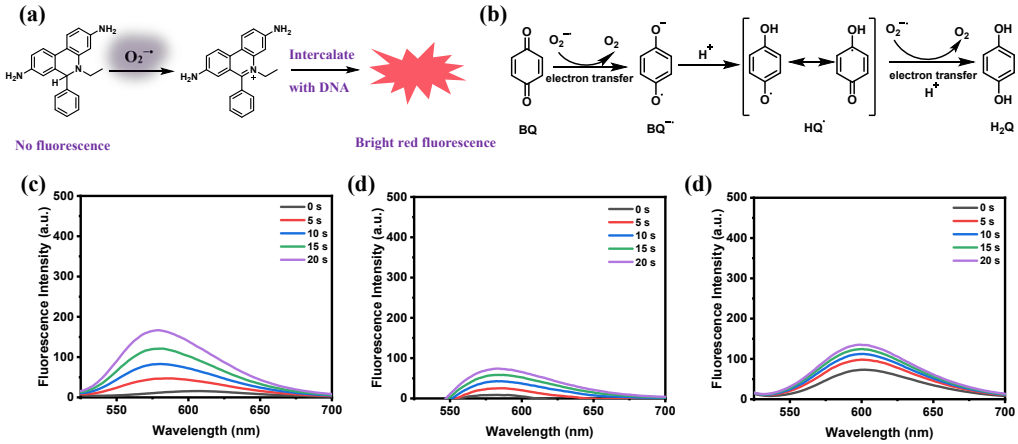

Figure S19. (a) The mechanism of dihydroethidium (DHE) as the $O_2^{-\bullet}$ probe; (b) The quenching mechanism of $O_2^{-\bullet}$ by 1,4-benzoquinone; The fluorescence spectra change of DHE solutions containing 500 μg/mL ctDNA upon irradiation (470 nm, 22.5 mW cm^{-2}) for different time in the presence of complex 2 (5 μM) (c), tpy-BODIPY (5 μM) (d), complex 1 (5 μM) and 1,4-benzoquinone (100 μM) (e).

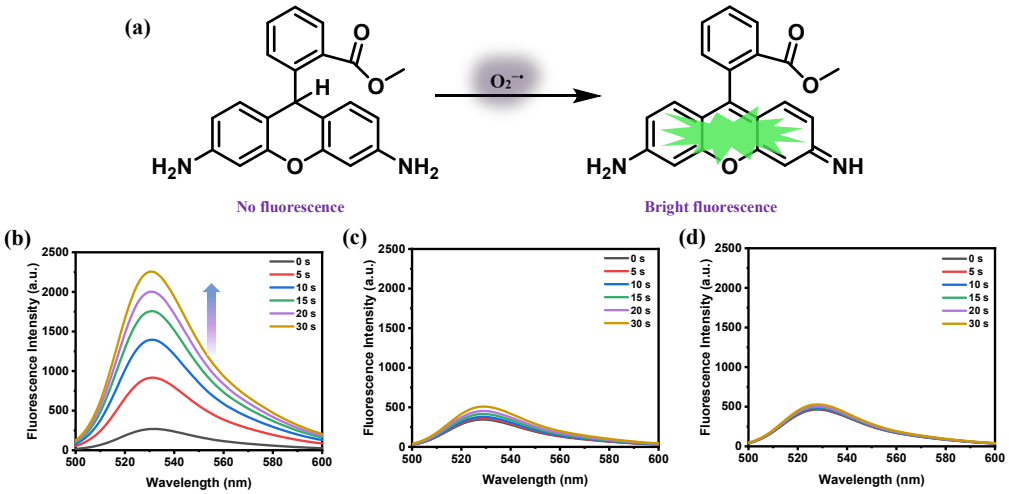

Figure S20. (a) The mechanism of DHR 123 as the $O_2^{-\bullet}$ probe; The fluorescence spectra of DHR 123 in H_2O upon irradiation (470 nm, 22.5 mW cm^{-2}) for different time in the presence of complex 1 (5 μM) (b), complex 2 (5 μM) (c) and none (control, d).

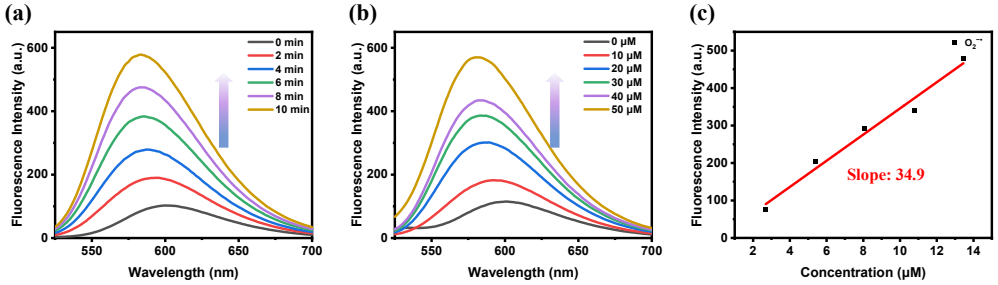

Figure S21. (a) Fluorescence spectra of DHE (20 μM) after irradiation (470 nm, 22.5 mW cm^{-2}) for different times in the presence of complex 1 (0.1 μM) in PBS; (b) Fluorescence spectra of DHE (20 μM) incubated with increasing concentrations of xanthine (0-50 μM) in the presence of xanthine oxidase (0.005 U ml^{-1}) in PBS. (c) The calibration curve of DHE fluorescence intensity to actual $O_2^{-\bullet}$ concentrations which was constructed using the xanthine/xanthine oxidase system combined with ferricytochrome c.

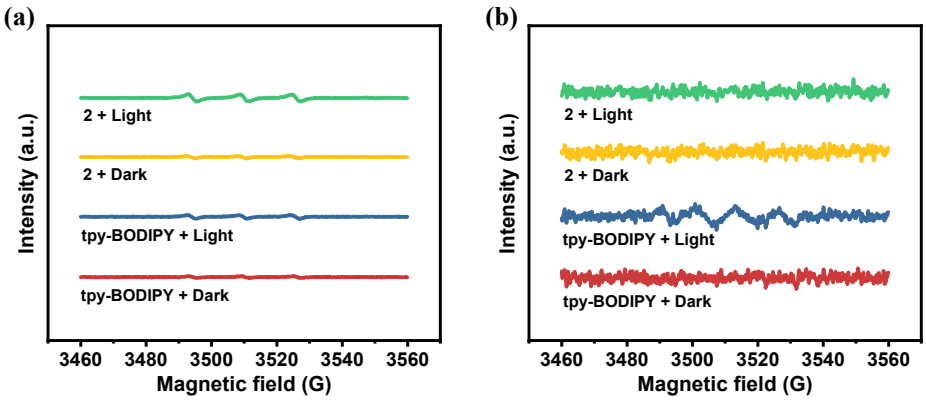

Figure S22. ESR spectra for detection of $^1O_2$ (a) and $O_2^{-\bullet}$ (b) in the presence of 2 or tpy-BODIPY in the dark or upon irradiation.

6. Photo-degradation of complex 1

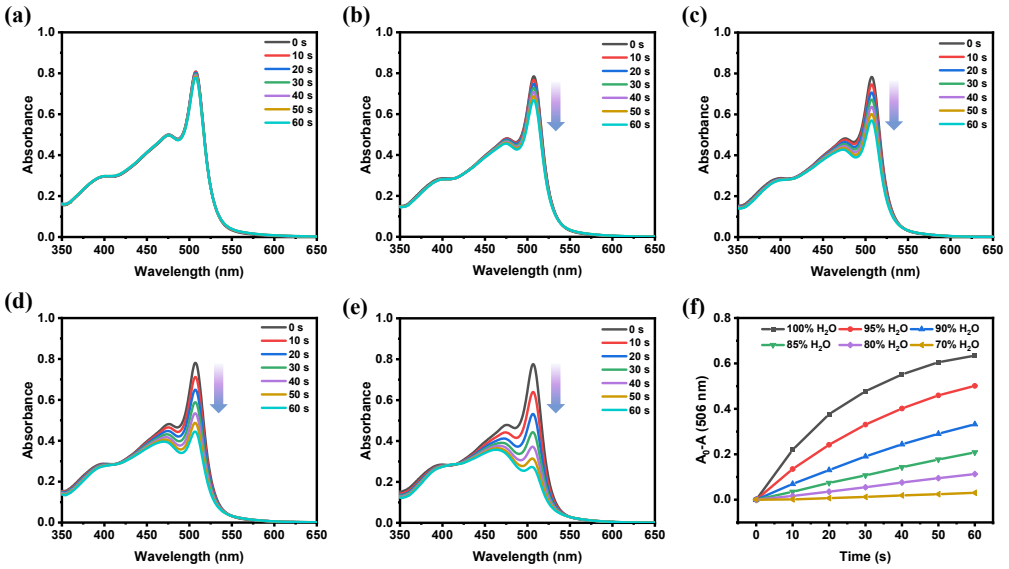

Figure S23. Absorption spectral changes of complex 1 upon irradiation (470 nm, 22.5 mW cm^{-2}) in solutions with different proportions of water and acetone. (a) 70% H_2O; (b) 80% H_2O; (c) 85% H_2O; (d) 90% H_2O; (e) 95% H_2O; (f) Plots of ΔAbs (A_0-A) at 506 nm of complex 1 in different solutions.

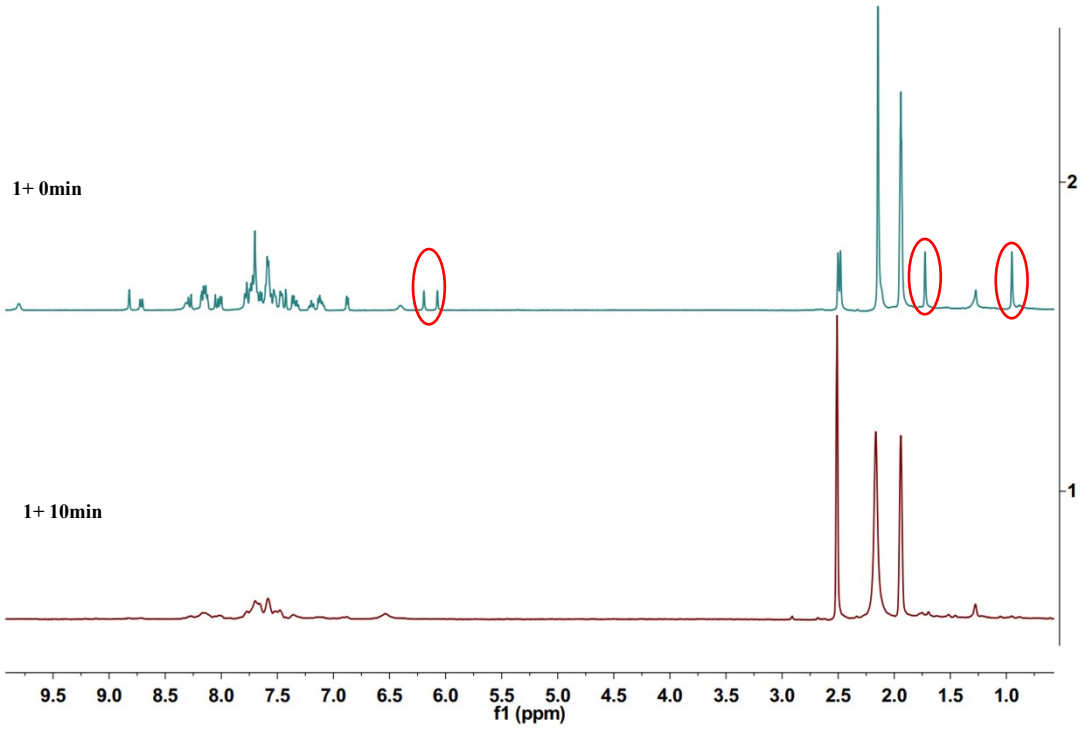

Figure S24. ^{1}H NMR spectra of complex 1 before (top) and after irradiation (470 nm, 22.5 mW cm^{-2}) for 10 min in H_2O (bottom). The spectra were recorded in CD_3CN. After irradiation, BODIPY based peaks at 6.20, 6.08, 1.73 and 0.96 ppm disappeared.

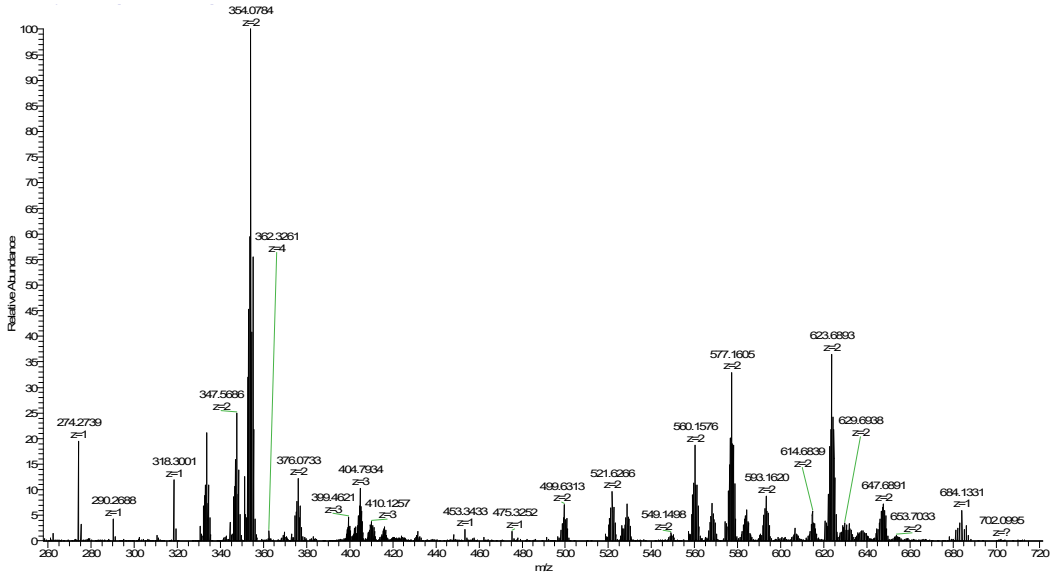

Figure S25. ESI mass spectrum of complex 1 in H_2O after light-irradiation (470 nm, 22.5 mW cm^{-2}, 10 min).

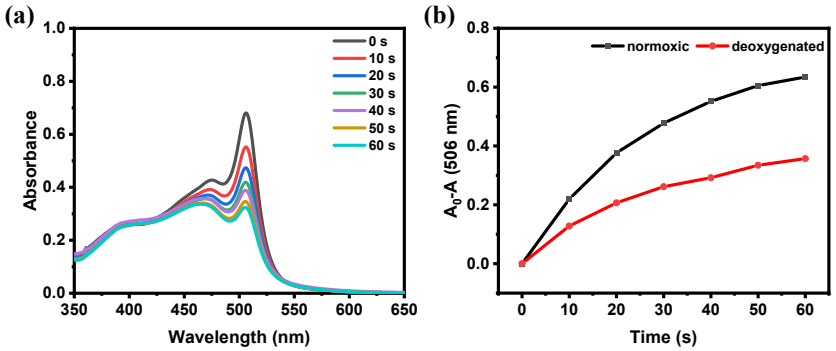

Figure S26. (a) Absorption spectral changes of complex 1 in degassed H_2O upon light-irradiation; (b) Plots of ΔAbs (A_0-A) at 506 nm of complex 1 in H_2O upon light-irradiation for different time intervals under normoxic and deoxygenated conditions.

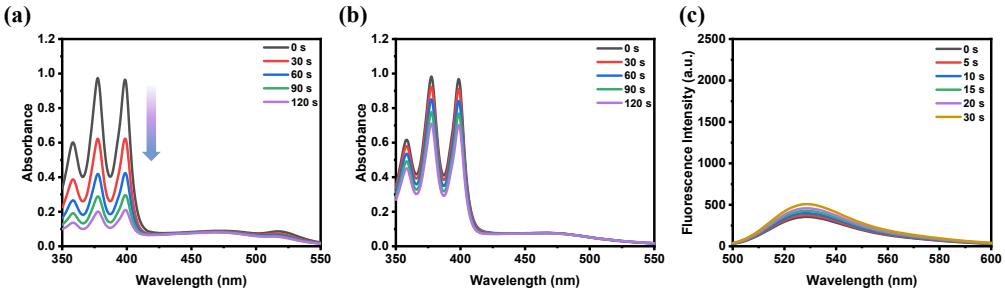

Figure S27. Absorption spectral changes of ABDA in H_2O after irradiation (470 nm, 22.5 mW cm^{-2}) for different time in the presence of complex 1 (a) and pre-irradiated (10 min in H_2O) complex 1 (b); (c) The fluorescence spectral changes of DHR 123 in H_2O after irradiation (470 nm, 22.5 mW cm^{-2}) for different time in the presence of pre-irradiated complex 1 (10 min in H_2O).

7. Experimental data in vitro

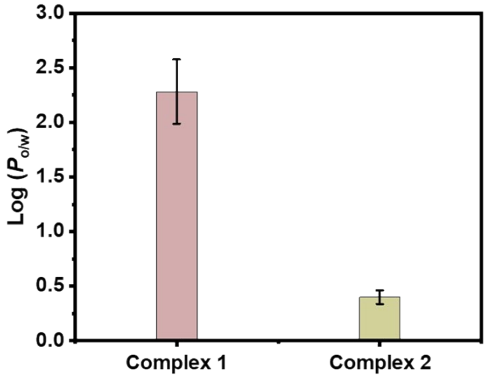

Figure S28. The *n*-octanol/water partition coefficients of complexes 1 and 2.

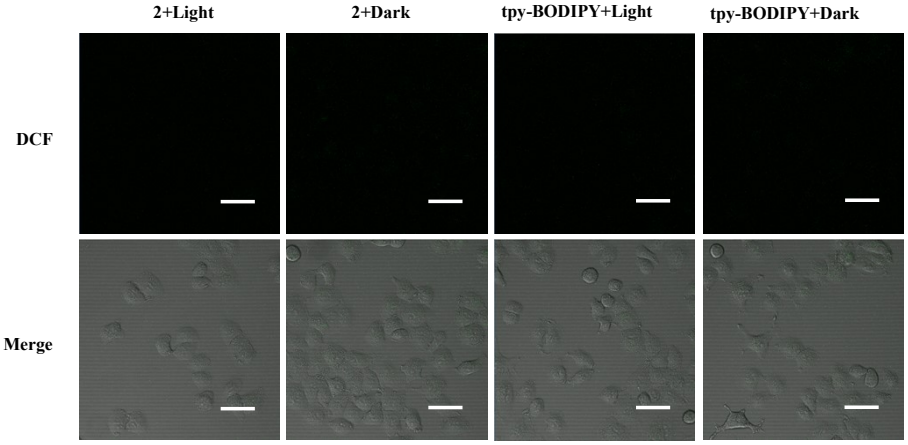

Figure S29. Detection of intracellular ROS production by DCFH-DA for A549 cells treated with complex 2 or tpy-BODIPY (0.1 μM) in the dark or upon irradiation (470 nm, 22.5 mW cm^{-2} for 10 min) under normoxic conditions. The scale bars represent 50 μm.

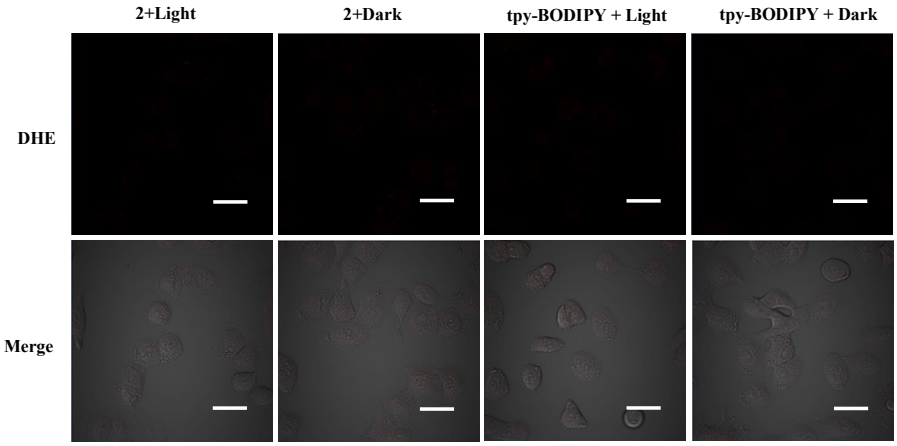

Figure S30. Detection of intracellular $O_2^{-\bullet}$ by DHE for A549 cells treated with complex 2 or tpy-BODIPY (0.1 μM) in the dark or upon irradiation (470 nm, 22.5 mW cm^{-2} for 10 min) under normoxic conditions. The scale bar represents 50 μm.

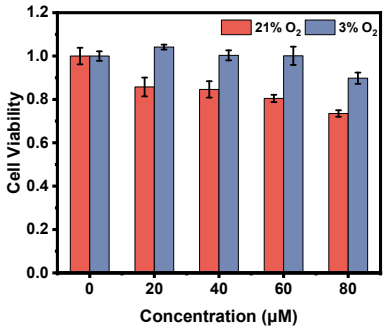

Figure S31. Cytotoxicity of complex 1 towards A549 cells in the dark under normoxic or hypoxic conditions.

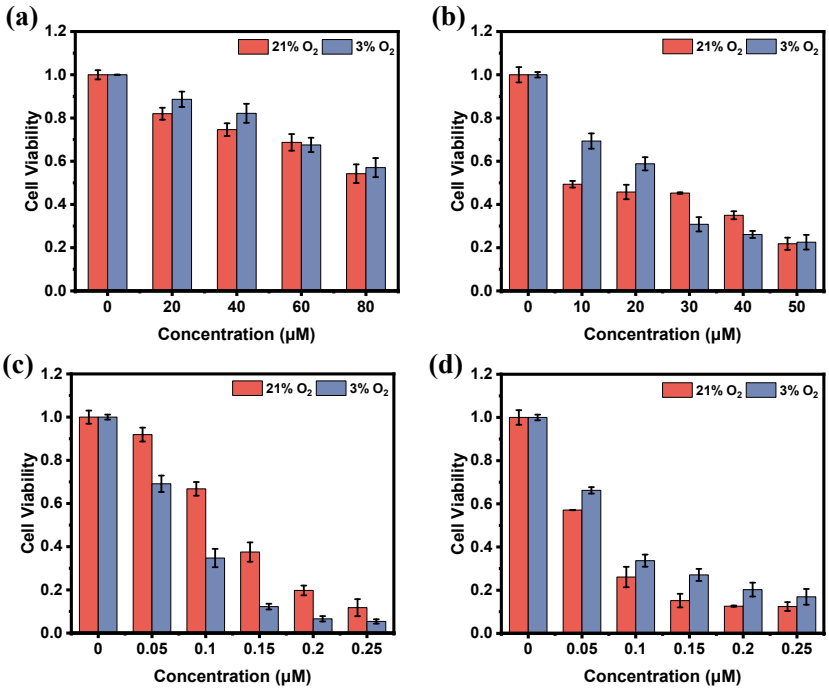

Figure S32. Cytotoxicity of complex 1 towards HeLa (a, c), B16-F10 (b, d) cells in the dark (a, b) or upon irradiation (470 nm, 22.5 mW cm^{-2} for 10 min) (c, d) under normoxic or hypoxic conditions.

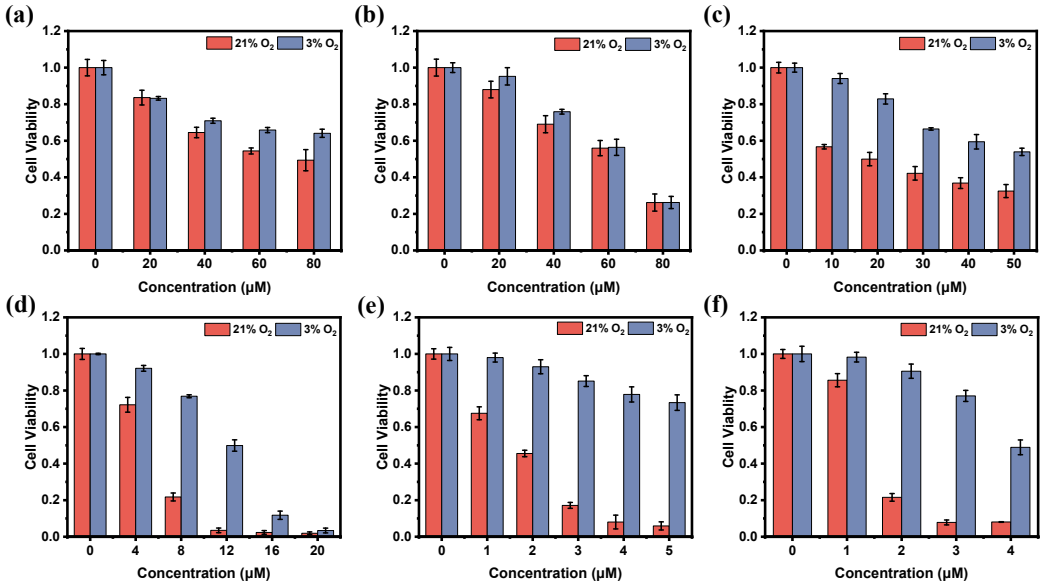

Figure S33. Cytotoxicity of complex 2 towards A549 (a, d), HeLa (b, e), B16-F10 (c, f) cells in the dark (a, b, c) or upon light-irradiation (470 nm, 22.5 mW cm^{-2} for 10 min) (d, e, f) under normoxic or hypoxic conditions.

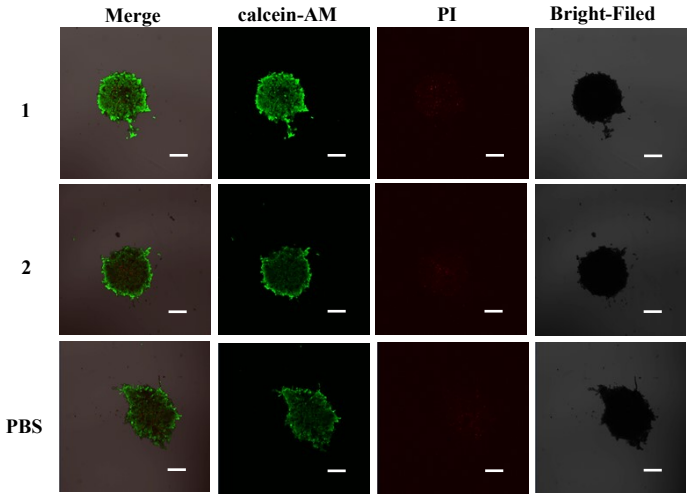

Figure S34. Calcein-AM and PI co-stained images of A549 3D MCSs treated with 1 or 2 (0.5 μM) or PBS without irradiation. Scale bars: 250 μm.

References

1 R. Joseph, A. Nkrumah, R. J. Clark and E. Masson, *J. Am. Chem. Soc.*, 2014, **136**, 6602-6607.

2 D. E. McCoy, T. Feo, T. A. Harvey and R. O. Prum, *Nat. Commun.*, 2018, **9**, 1.

3 Q. X. Zhou, W. H. Lei, Y. Sun, J. R. Chen, C. Li, Y. J. Hou, X. S. Wang and B. W. Zhang, *Inorg. Chem.*, 2010, **49**, 4729-4731.

4 C. Lee, W. Yang and R. G. Parr, *Phys. Rev. B*, 1988, **37**, 785-789.

5 L. E. Roy, P. J. Hay and R. L. Martin, *J. Chem. Theory. Comput.*, 2008, **4**, 1029-1031.

6 M. M. Francl, W. J. Pietro, W. J. Hehre, J. S. Binkley, M. S. Gordon, D. J. DeFrees and J. A. Pople, *J. Chem. Phys.*, 1982, **77**, 3654-3665.

7 P. C. Hariharan and J. A. Pople, *Theoret. Chim. Acta*, 1973, **28**, 213-222.